Self-assembled copper(II) metallacycles derived from asymmetric Schiff base ligands: Efficient host for ADP/ATP in phosphate buffer

Amit Kumar[†], Rampal Pandey[†], Ashish Kumar[†], Rakesh Kumar Gupta[†], Mrigendra Dubey[†], Akbar Mohammed[‡], Shaikh M. Mobin[‡], and Daya Shankar Pandey[†*]

[†]*Department of Chemistry, Faculty of Science, Banaras Hindu University, Varanasi - 221 005, India*

[‡]*Discipline of Chemistry, Indian Institute of Technology, Indore - 452 017, India*

Supporting Information Placeholder

Contents:

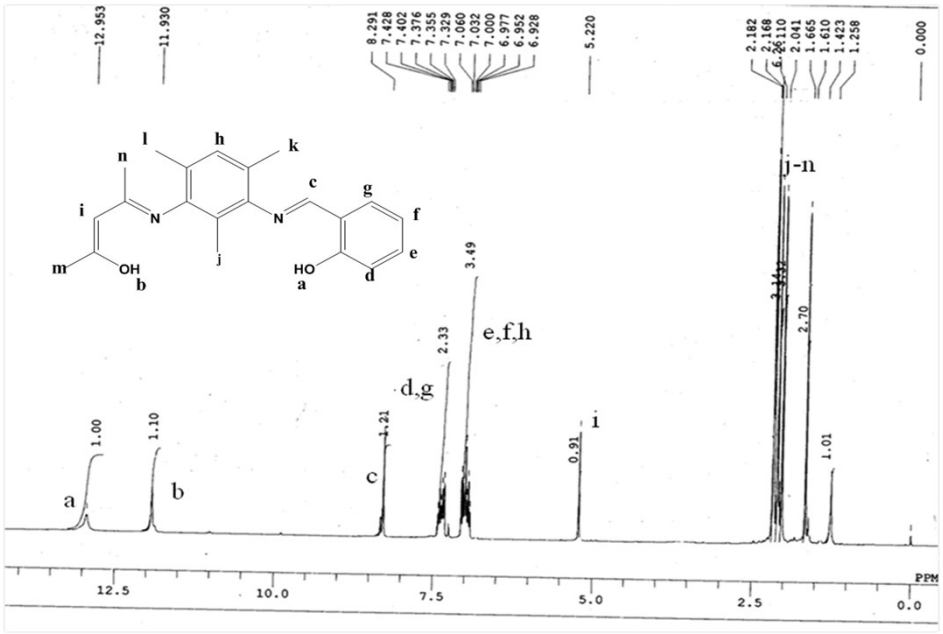

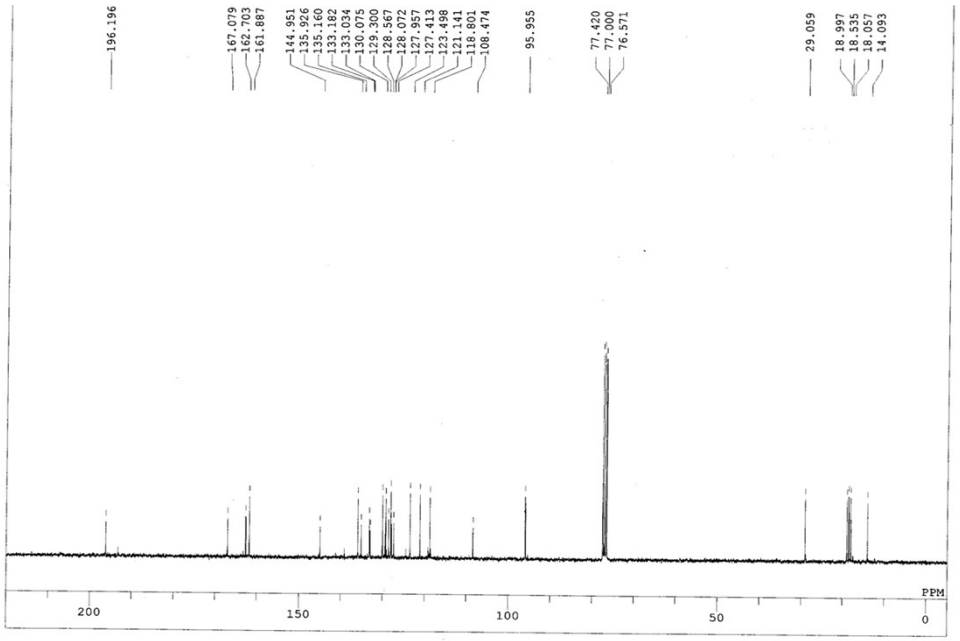

Fig. S1 ^{1}H (above) and ^{13}C (below) NMR spectra of $\mathbf{H_2L^1}$.

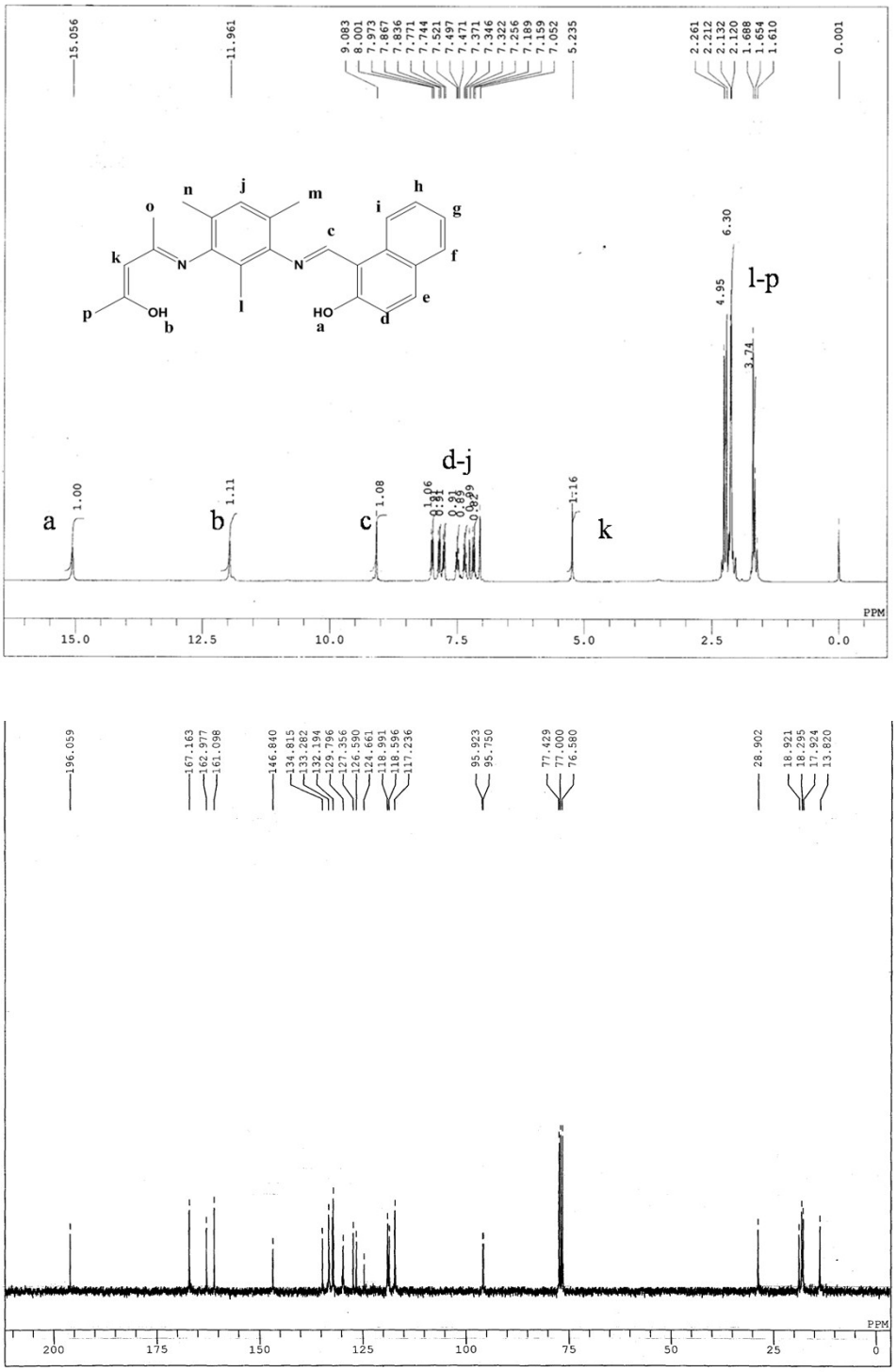

Fig. S2 ^{1}H (above) and ^{13}C (below) NMR spectra of $\mathbf{H_2L^2}$.

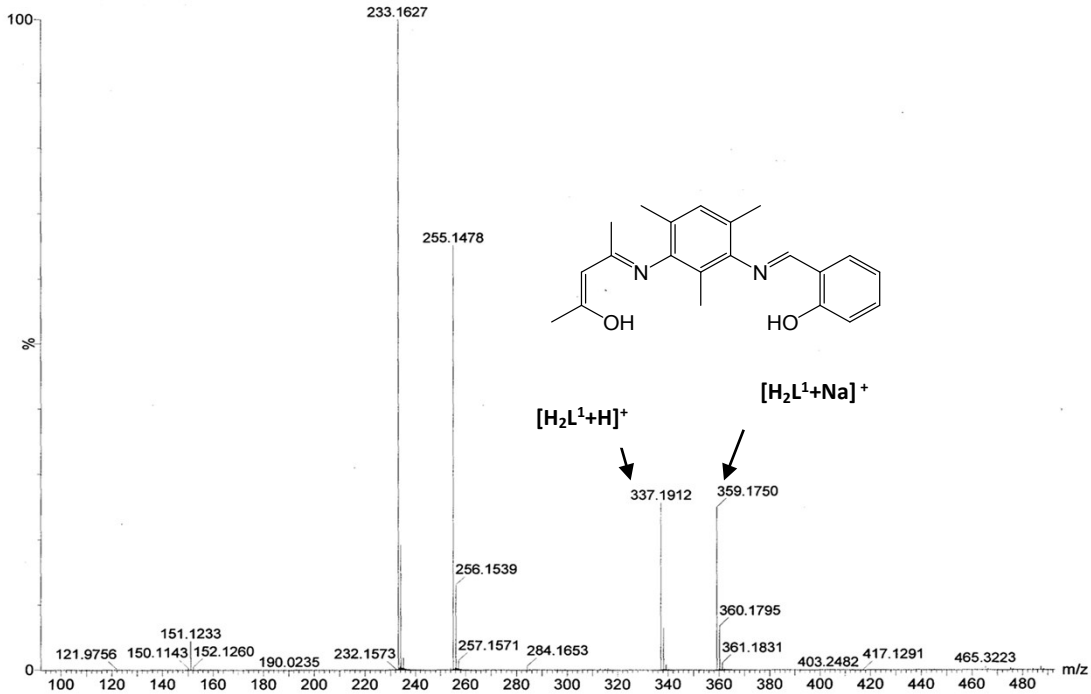

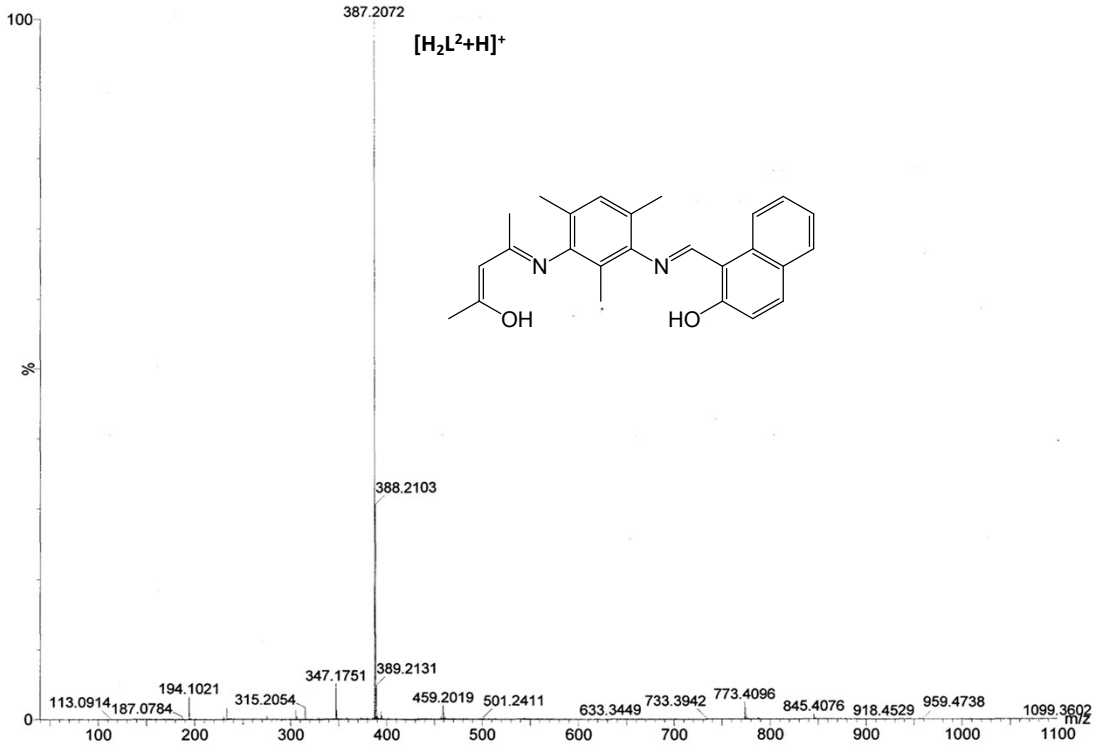

Fig. S3 ESI-Mass spectra of $\mathbf{H_2L^1}$ (above) of $\mathbf{H_2L^2}$ (below).

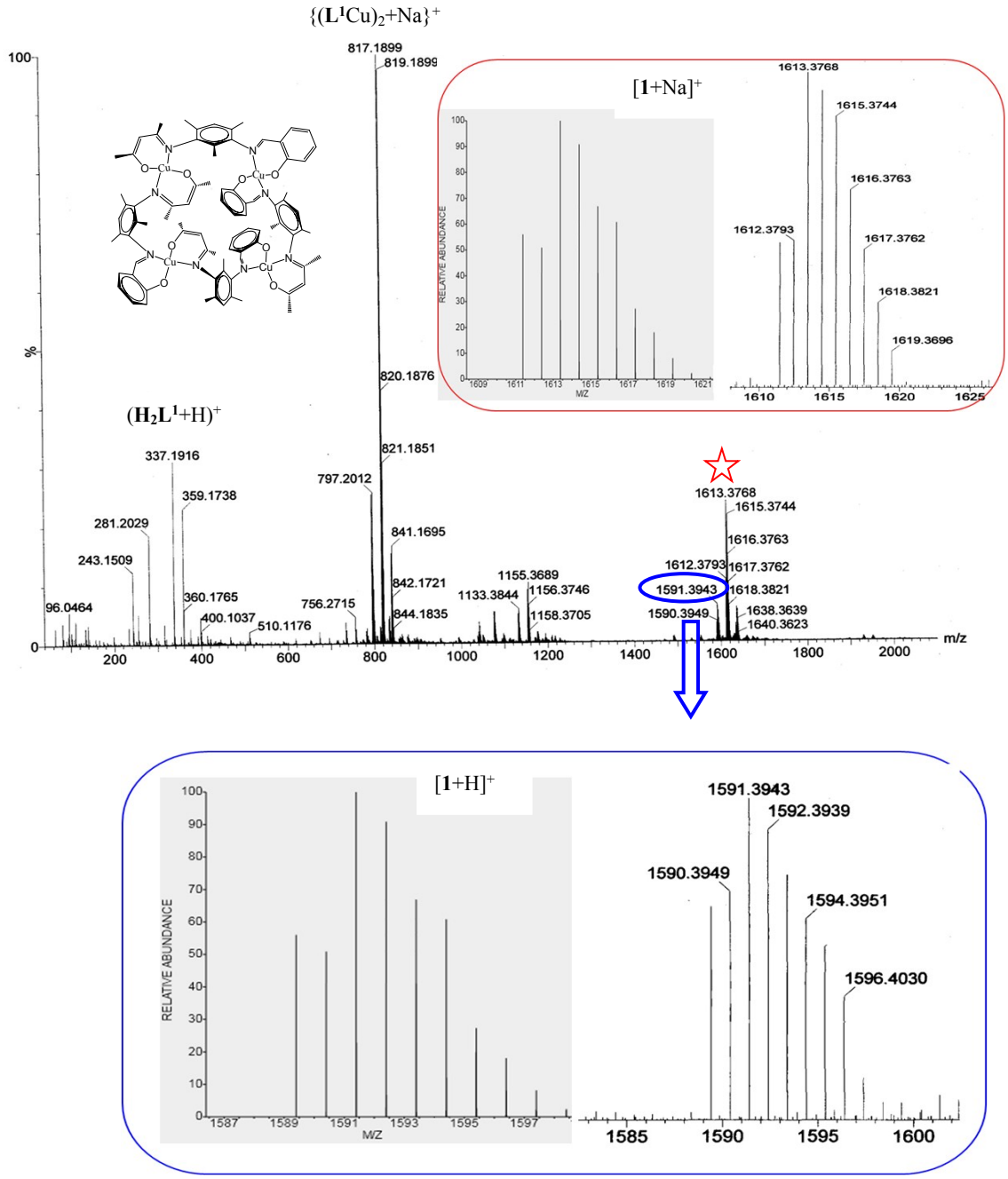

Fig. S4 ESI-Mass spectrum of **1**. Simulated isotopic pattern for the molecular ion peak at *m/z* 1613.3768 $[M+Na]^+$ (red circle, inset) and 1591.3943 $[M+H]^+$ (blue circle, below).

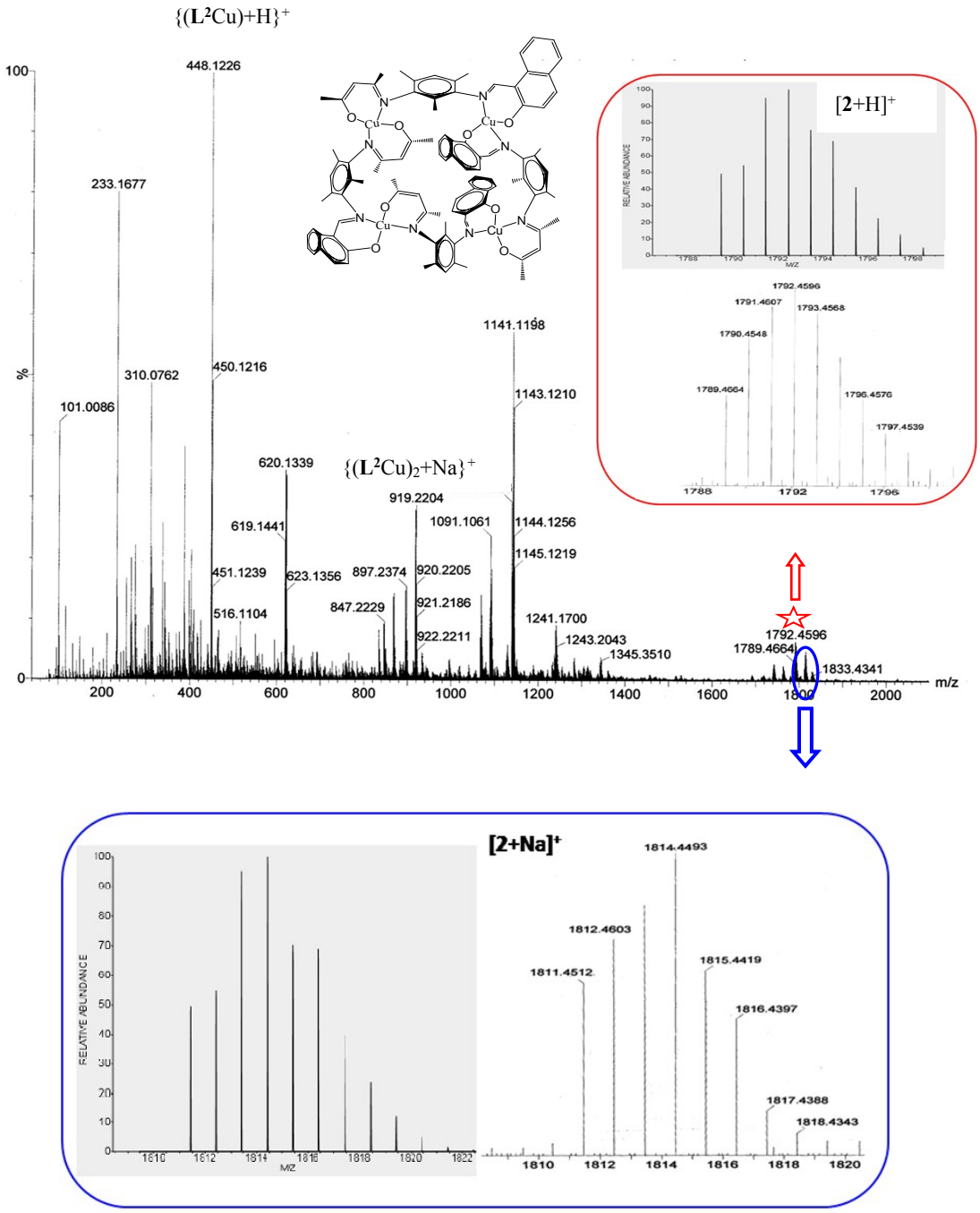

Fig. S5 ESI-Mass spectrum of **2**. Simulated isotopic pattern for the molecular ion peak at *m/z* 1792.4596 {$[M+H]^+$ (red circle, inset) and 1814.4493 $[M+Na]^+$ (blue circle, below).

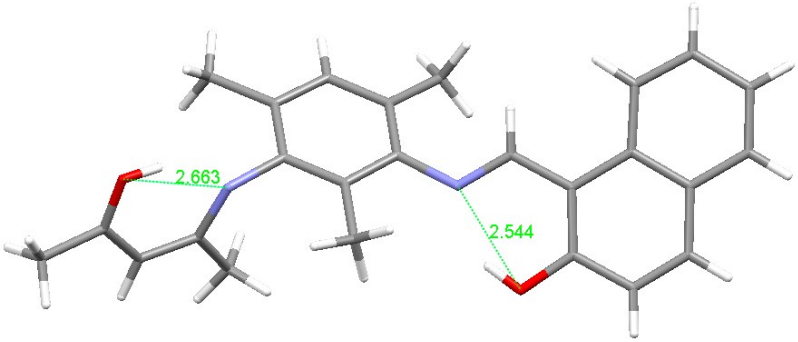

Fig. S6 Intra-molecular hydrogen bonding interactions in $\mathbf{H_2L^2}$.

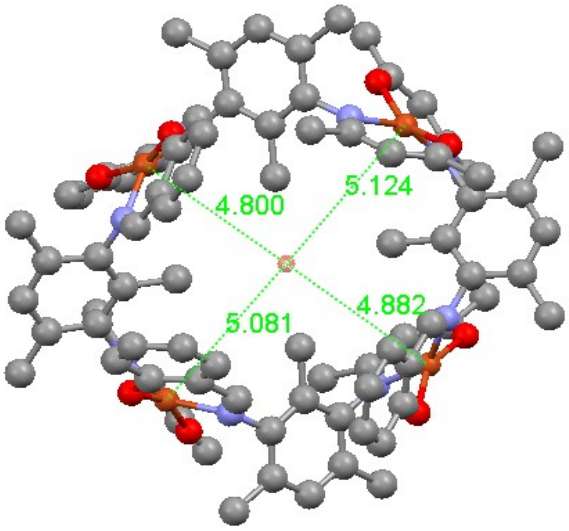

Fig. S7 Crystal structure of **1** showing distances from centroid of cavity to Cu(II) centre.

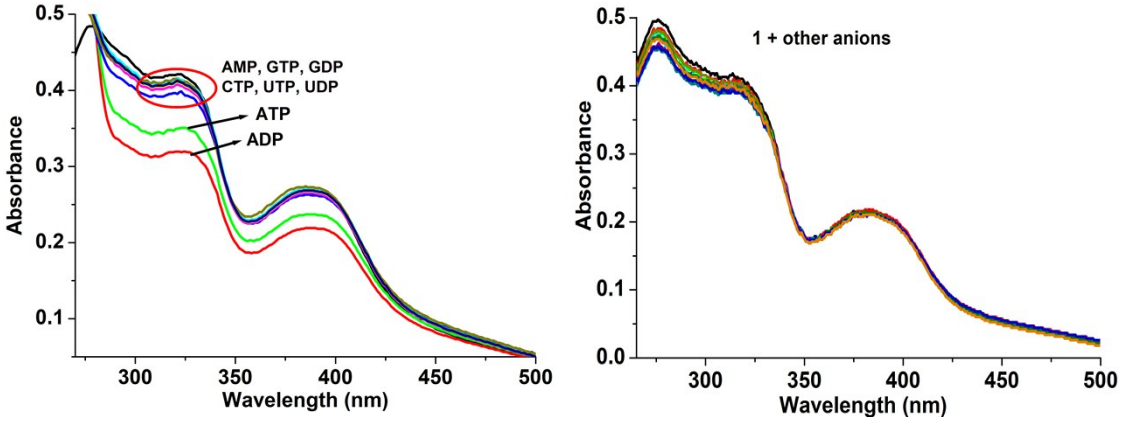

(a) (b)

Fig. S8 UV/vis spectra of **1** in presence of various NPPs [ATP, ADP, AMP, GTP, GDP, CTP, UTP and UDP (a)] and anions [F^-, Cl^-, Br^-, I^-, SO_4^{2-}, S^{2-}, HSO_3^-, SO_3^{2-}, $S_2O_3^{2-}$, $S_2O_8^{2-}$, CO_3^{2-}, NO_2^-, NO_3^-, $H_2PO_4^-$, HPO_4^{2-}, PO_4^{3-}, $P_2O_7^{4-}$ (b)].

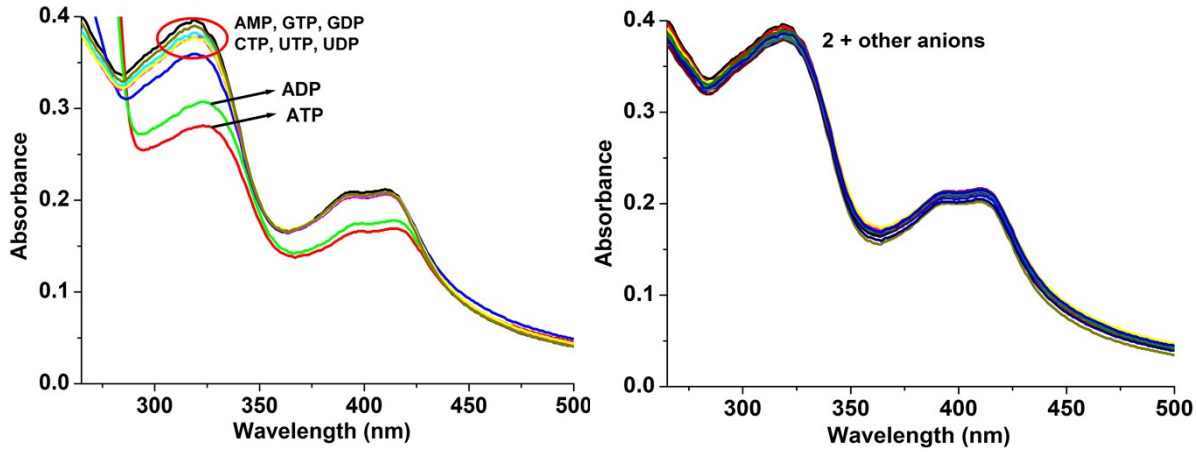

(a) (b)

Fig. S9 UV/vis spectra of **2** in presence of various NPPs [ATP, ADP, AMP, GTP, GDP, CTP, UTP and UDP (a)] and anions [F^-, Cl^-, Br^-, I^-, SO_4^{2-}, S^{2-}, HSO_3^-, SO_3^{2-}, $S_2O_3^{2-}$, $S_2O_8^{2-}$, CO_3^{2-}, NO_2^-, NO_3^-, $H_2PO_4^-$, HPO_4^{2-}, PO_4^{3-}, $P_2O_7^{4-}$ (b)].

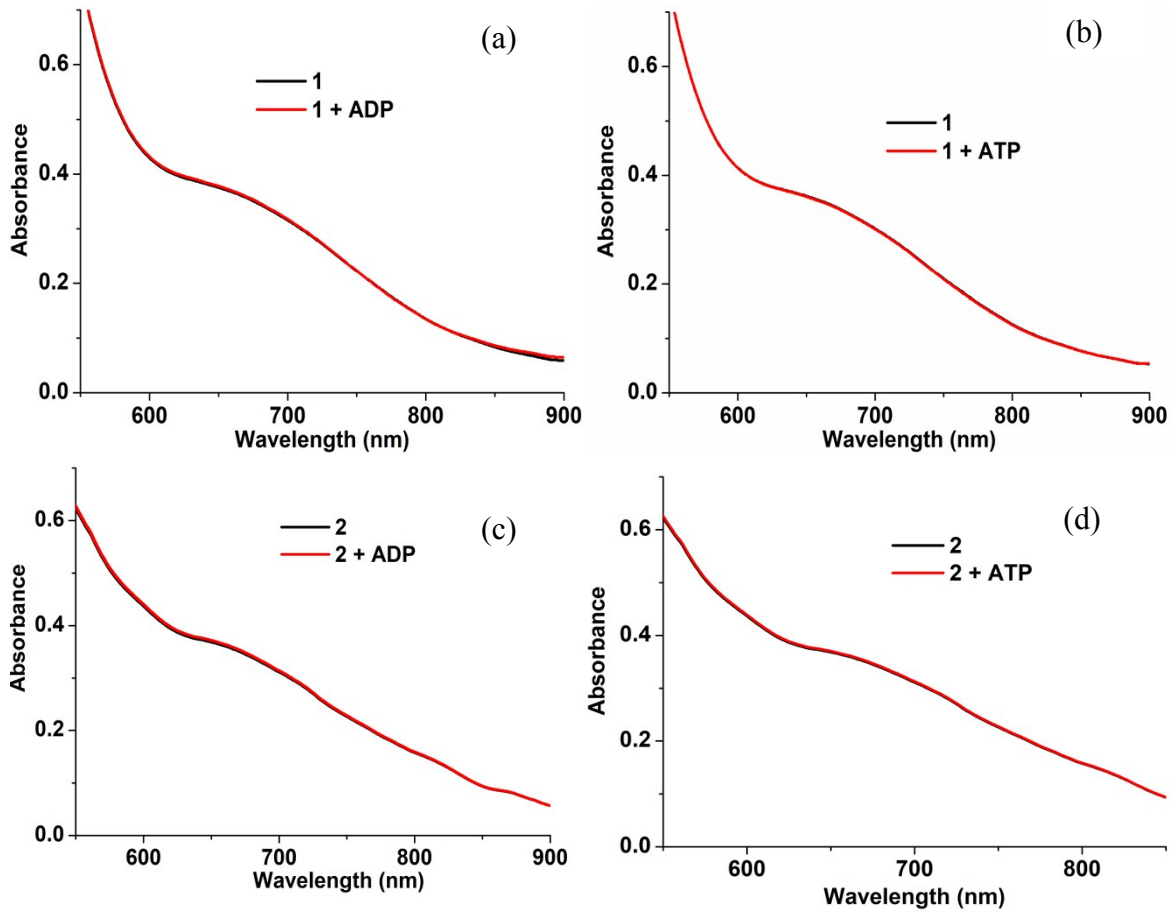

Fig. S10 UV/vis spectra of **1** and **2** (c, 1×10^{-3} M, DMSO/PBS, v/v, 1:99) showing d-d transition band in absence (black line) and presence (red line) of ADP/ATP (5.0 equiv).

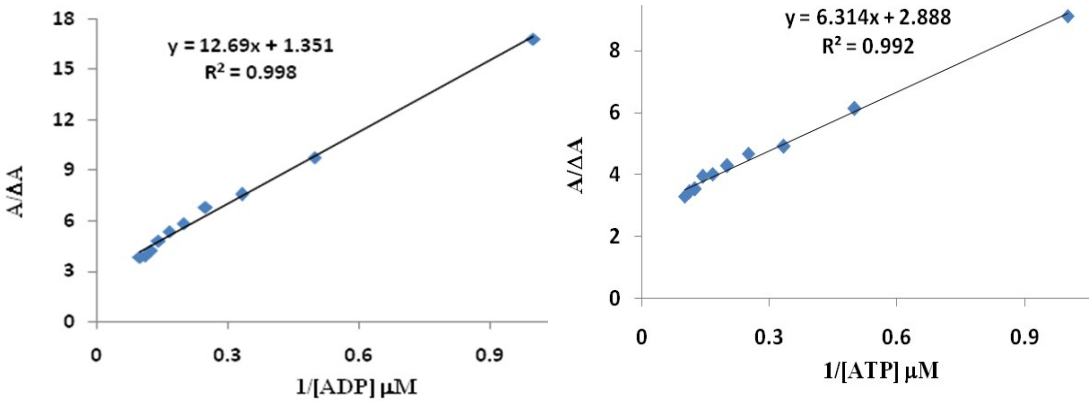

(a) (b)

Fig. S11 Estimation of association constant by Benesi-Hildebrand (B-H) plot for 1:1 stoichiometry for complexes between **1** + ADP (a) and **1** + ATP (b).

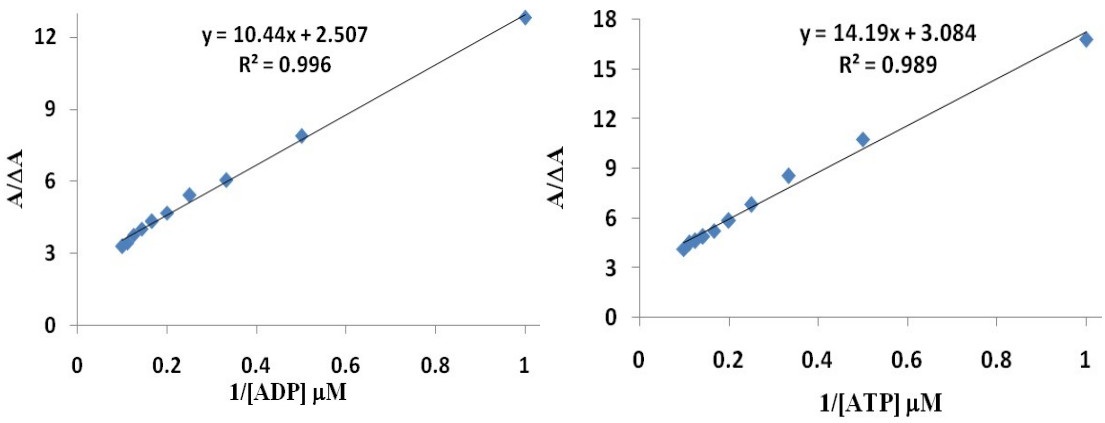

(a) (b)

Fig. S12 Estimation of association constant by Benesi-Hildebrand (B-H) plot for 1:1 stoichiometry for complexes between **2** + ADP (a) and **2** + ATP (b).

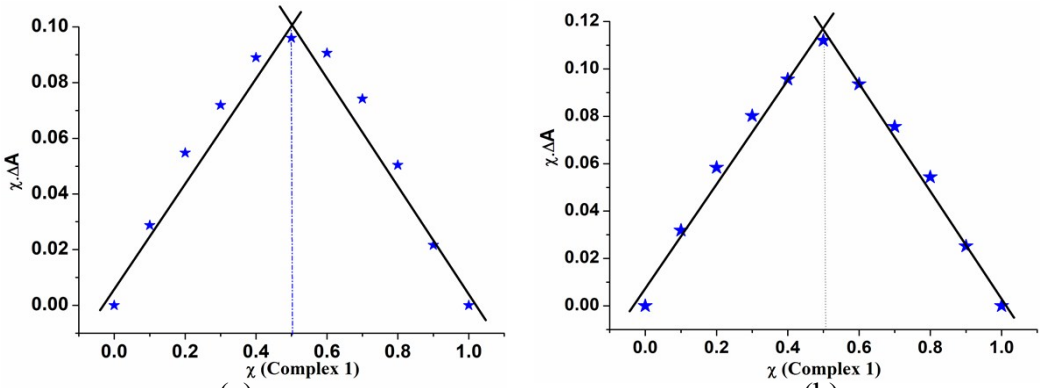

(a) (b)

Fig. S13 Job's plot analysis illustrating 1:1 stoichiometry for **1** with ADP (a) and ATP (b) from UV/vis spectra.

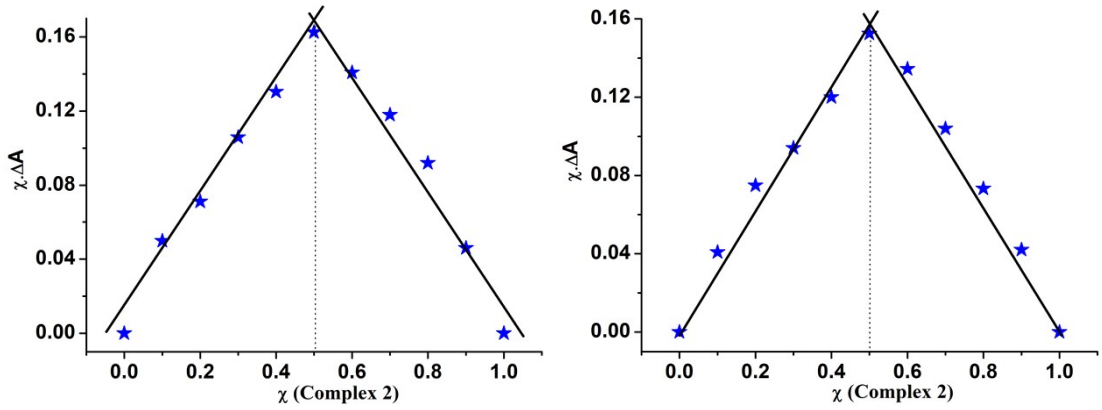

(a) (b)

Fig. S14 Job's plot analysis illustrating 1:1 stoichiometry for **2** with ADP (a) and ATP (b) from UV/vis spectra.

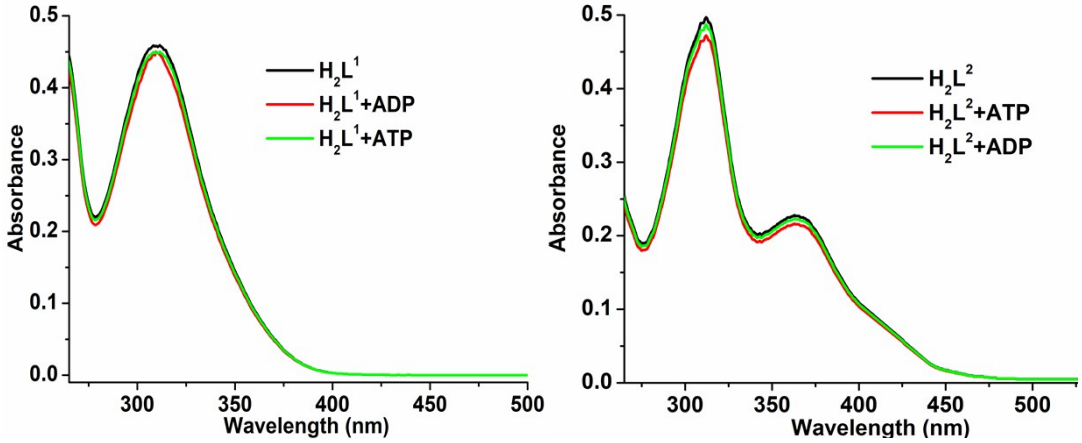

(a) (b)

Fig. S15 UV/vis spectra of $\mathbf{H_2L^1}$ (a) and $\mathbf{H_2L^2}$ (b), showing insignificant changes in presence of ADP/ATP.

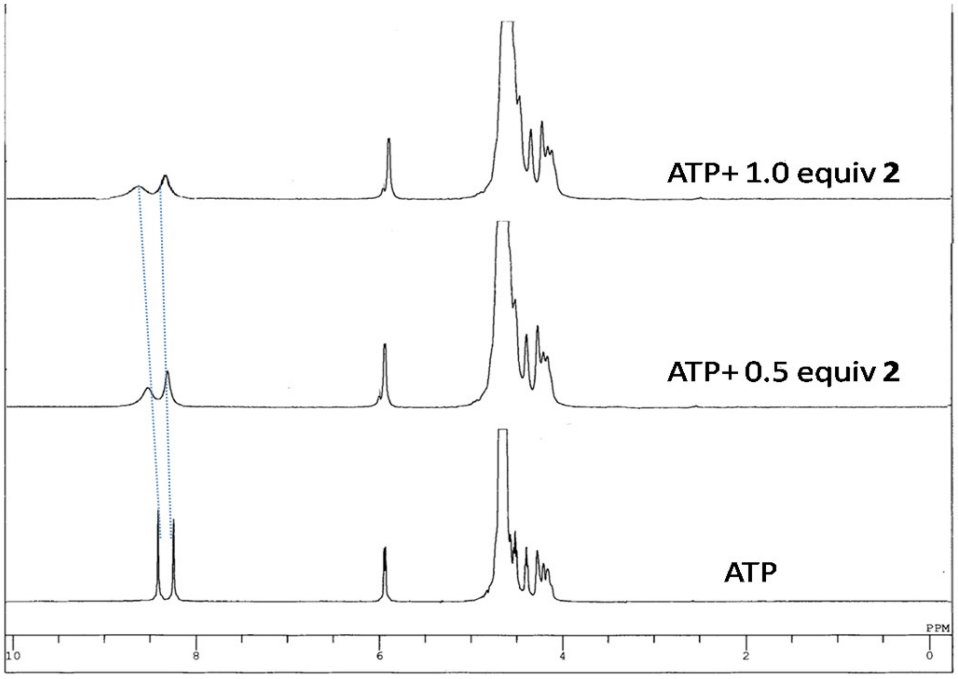

Fig. S16 ^{1}H NMR titration spectra for ATP (D_2O) with varying amount of **2** (blue dotted lines show downfield shifting in *H*8 and *H*2 adenine protons).

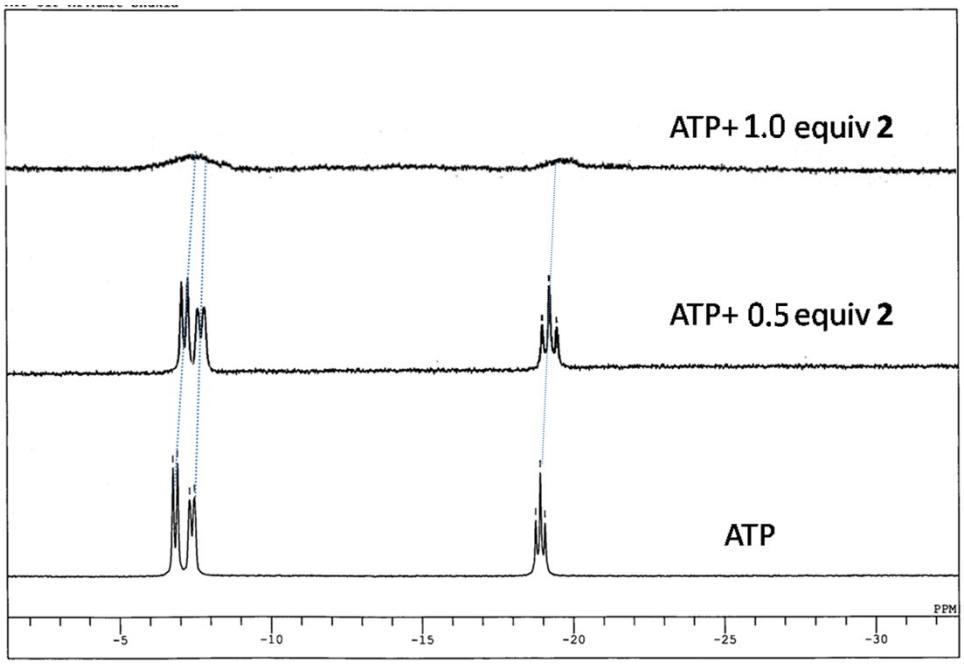

Fig. S17 ^{31}P NMR titration spectra of ATP (D_2O) with varying amount of **2** (blue dotted lines show upfield shifting in ^{31}P signals).

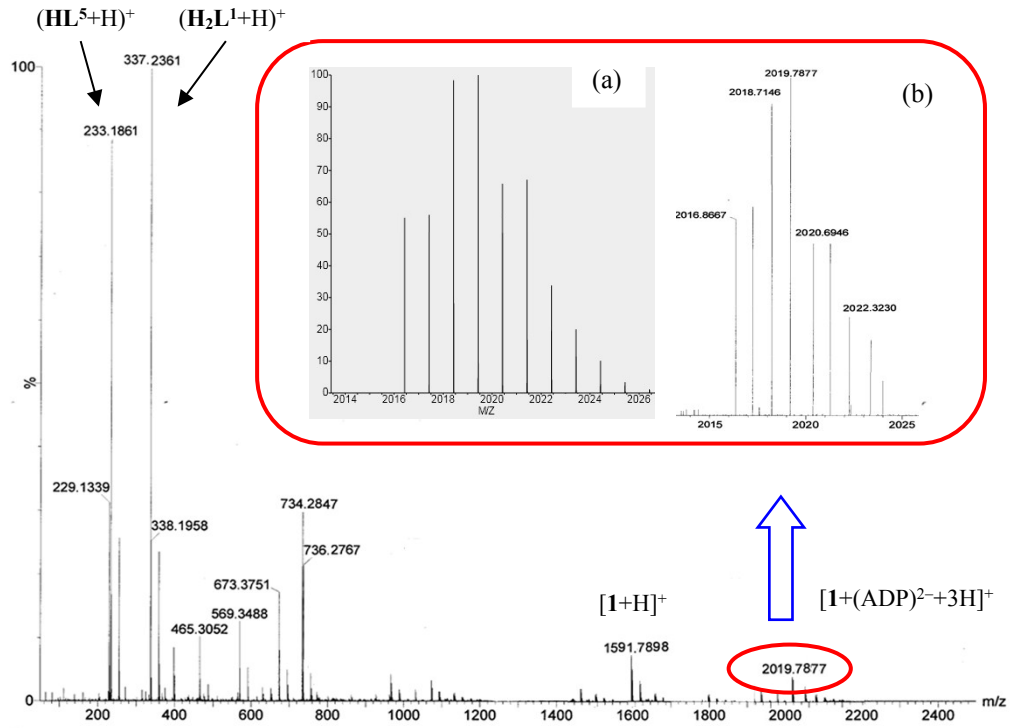

Fig. S18 ESI-MS of **1** + ADP [Inset shows simulated isotopic pattern for molecular ion peak at *m/z* 2019.7877 {**1** + $(ADP)^{2-}$ + 3H}$^{+}$].

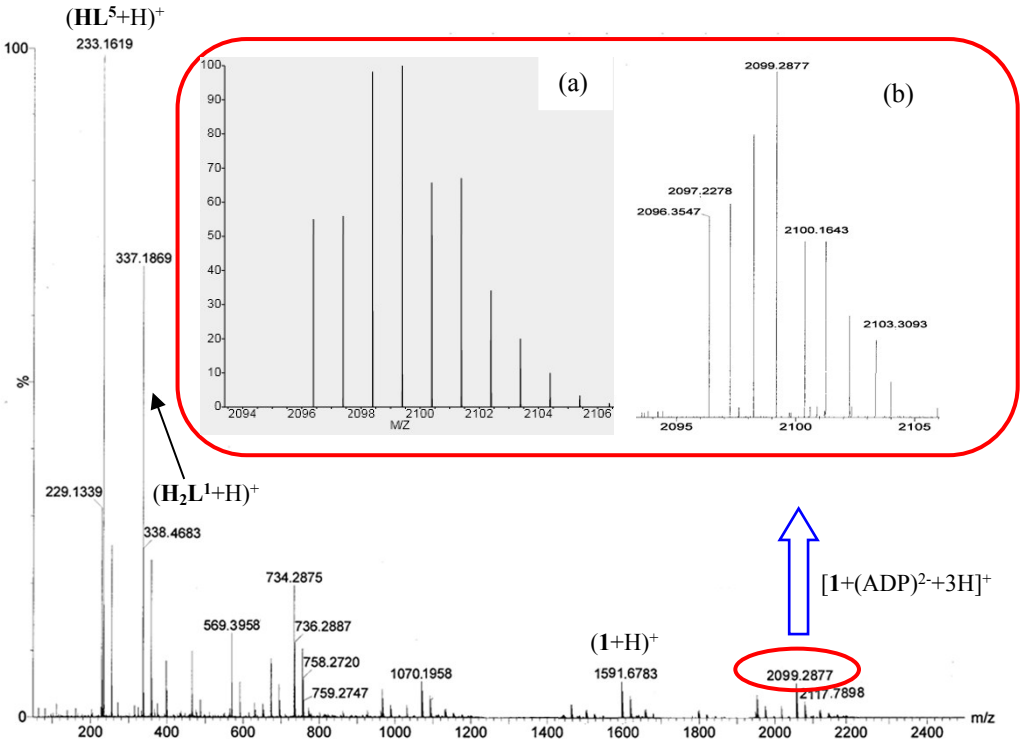

Fig. S19 ESI-MS of **1**+ATP [Inset shows simulated isotopic pattern for molecular ion peak at *m/z* 2099.2877 {**1** + $(ATP)^{2-}$ + 3H}$^{+}$].

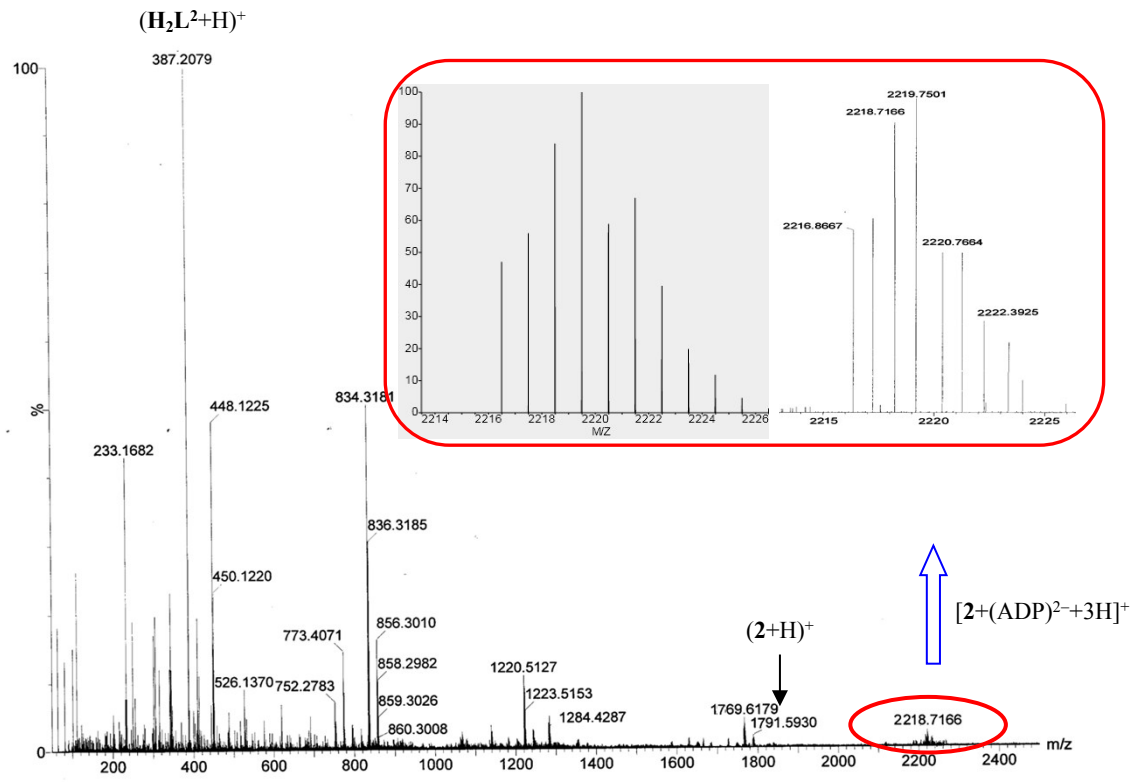

Fig. S20 ESI-MS of **2** + ADP [Inset showing simulated isotopic pattern for molecular ion peak at *m/z* 2219.7501 {**2** + $(ADP)^{2-}$ + 3H}$^{+}$].

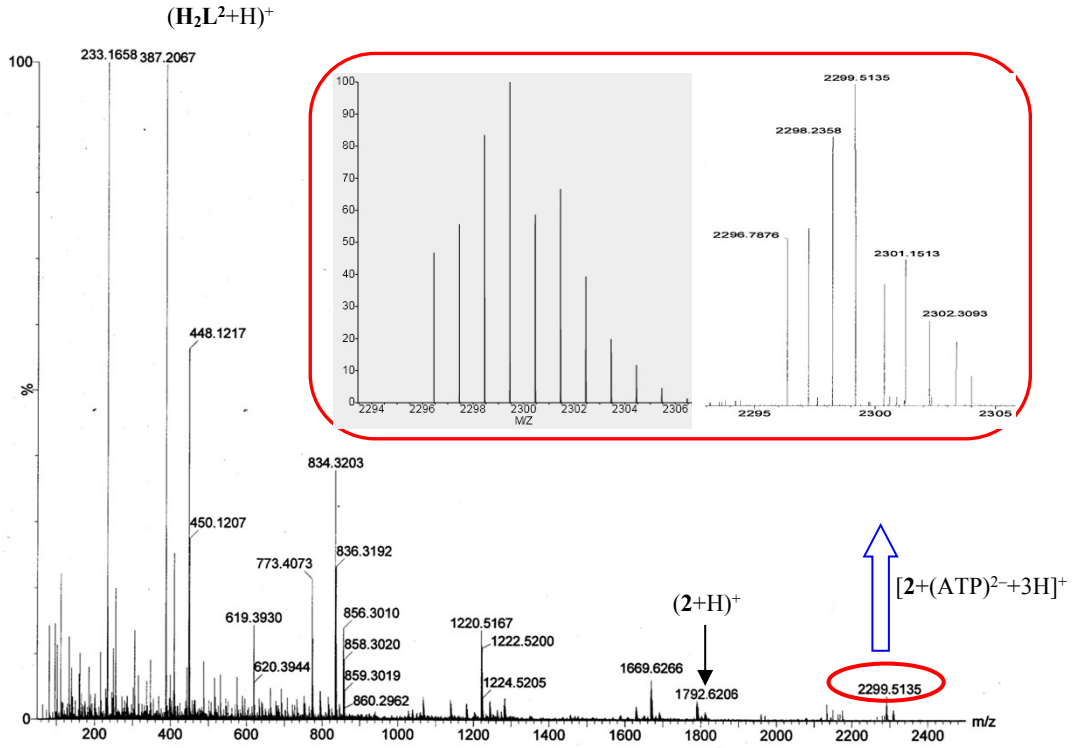

Fig. S21 ESI-MS of **2** + ATP [Inset showing simulated isotopic pattern for molecular ion peak at *m/z* 2299.5135 {**2** + $(ATP)^{2-}$ + 3H}$^{+}$].

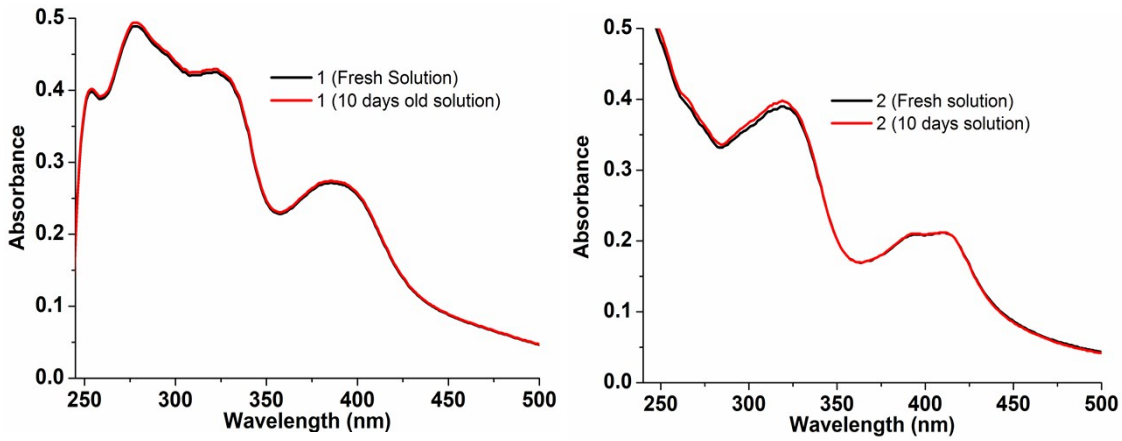

(a) (b)

Fig. S22 UV/vis spectra for a fresh (black line) and 10 days old solution (red line) for **1** (a) and **2** (b) (c, 10 μM, DMSO/PBS; v/v, 1:99).

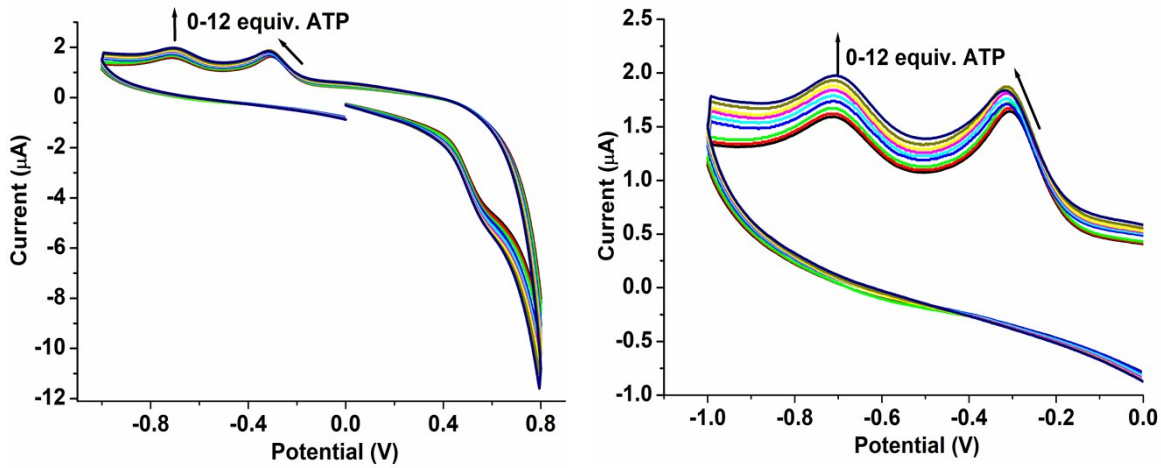

(a) (b)

Fig. S23 Cyclic voltammetric titration plots for **1** with increasing amount of ATP (0.0–12.0 equiv) in full window (a) and only in reduction window (b).

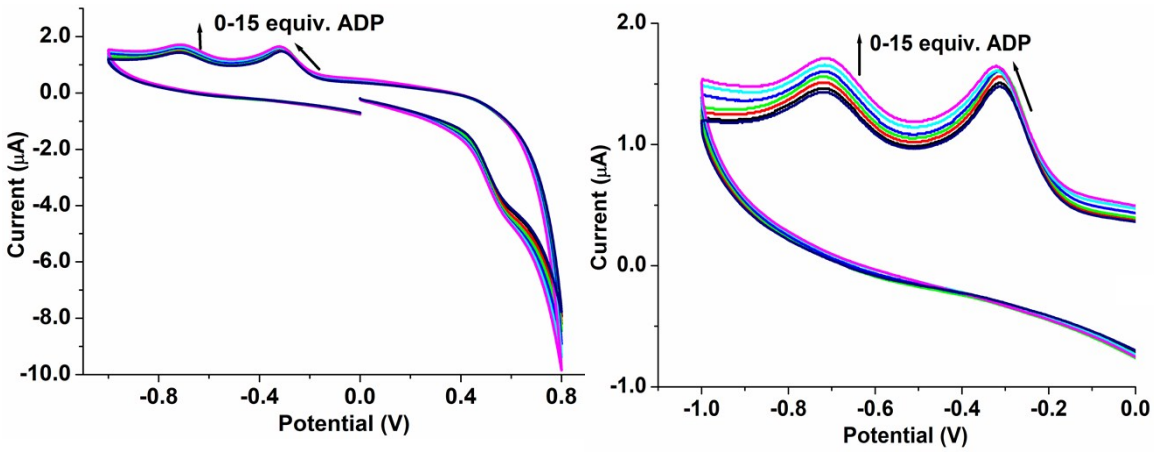

(a) (b)

Fig. S24 Cyclic voltammetric titration plots for **2** with increasing amount of ADP (0.0–15.0 equiv) in full window (a) and only in reduction window (b).

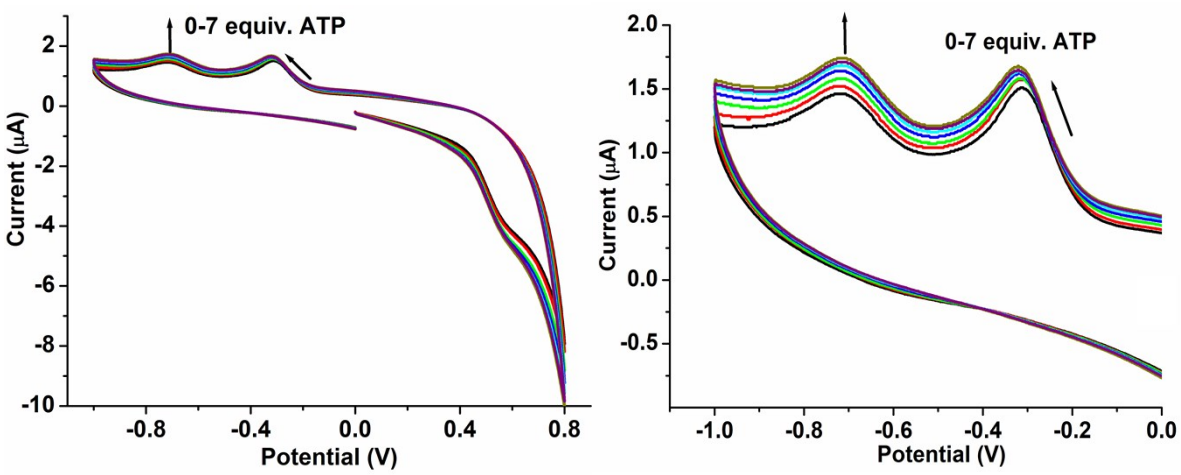

(a) (b)

Fig. S25 Cyclic voltammetric titration plots for **2** with increasing amount of ATP (0.0–7.0 equiv) in full window (a) and only in reduction window (b).

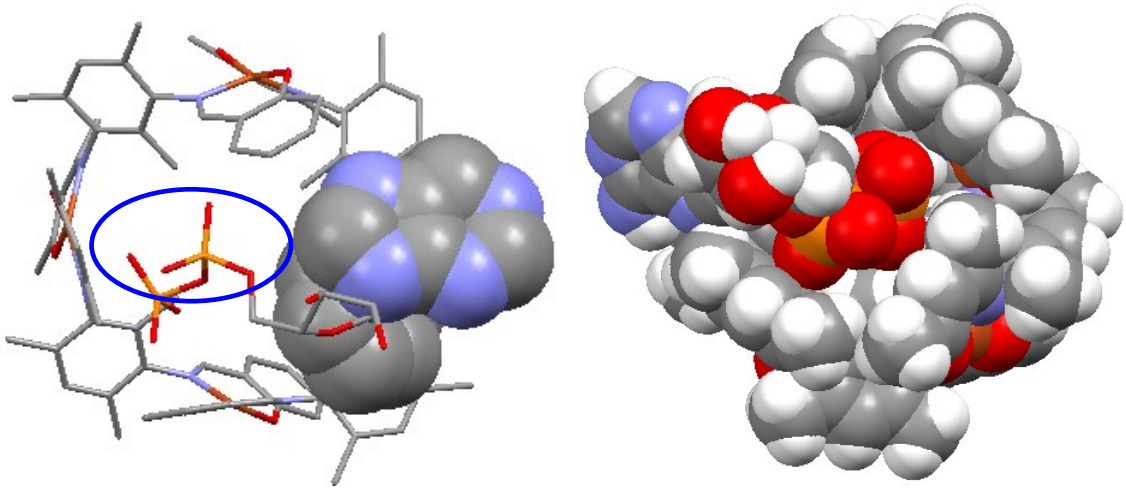

(a) (b)

Fig. S26 Molecular docked structures for **1** + ADP, show π–π interactions between adenine and salen core (a) and insertion of phosphate chain into the cavity shown by blue circle in (a) and space fill model in (b).

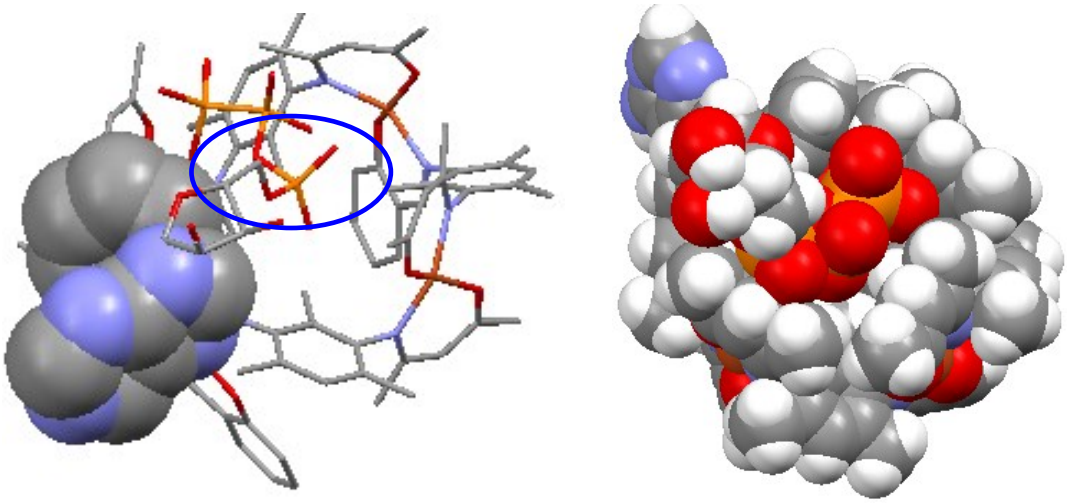

(a) (b)

Fig. S27 Molecular docked structures for **1** + ATP, show π–π interactions between adenine and salen core (a) and insertion of phosphate chain into the cavity shown by blue circle in (a) and space fill model (b).

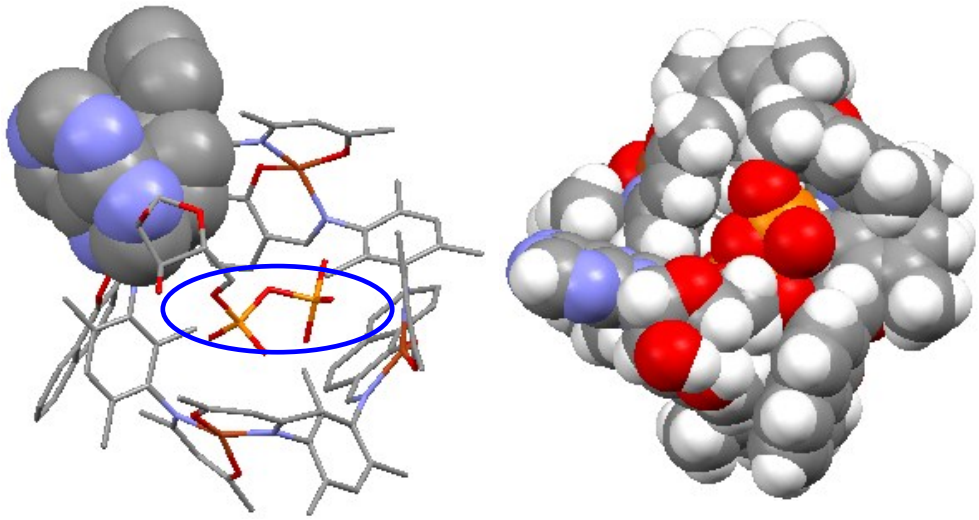

(a) (b)

Fig. S28 Molecular docked structures for **2** + ADP, show π–π interactions between adenine and salen core (a) and insertion of phosphate chain into the cavity shown by blue circle in (a) and space fill model (b).

Table S1. UV/vis data of $\mathbf{H_2L^1}$, $\mathbf{H_2L^2}$, **1** and **2**.

$\mathbf{H_2L^1}$	310 (ε, 4.57 × 10^4) and 262 nm (ε, 4.41 × 10^4)
$\mathbf{H_2L^2}$	364 (ε, 2.26 × 10^4) and 312 nm (ε, 4.94 × 10^4)
1	386 (ε, 2.69 × 10^4) and 323 nm (ε, 4.21 × 10^4)
2	410 (ε, 2.14 × 10^4) and 319 nm (ε, 3.94 × 10^4)

Table S2 Cyclic voltammetric data of $\mathbf{H_2L^1}$, $\mathbf{H_2L^2}$, **1** and **2**.

Compounds	Oxidation Potential; V (Current Density; μA)	Reduction Potential; V (Current Density; μA)
$\mathbf{H_2L^1}$	0.403 (I = –4.86)	---
$\mathbf{H_2L^2}$	0.382 (I = –4.50)	---
1	0.564 (I = –4.15)	–0.306V (I = 1.671) –0.719V (I = 1.620)
2	0.554 (I = –3.66)	–0.314V (I = 1.509) –0.717V (I = 1.465)

Table S3 Cyclic voltammetric data of **1** and **2** upon addition of ATP and ADP.

	Probe Reduction Potential; V (Current Density; μA)	Probe + ATP Reduction Potential; V (Current Density; μA)	Probe + ADP Reduction Potential; V (Current Density; μA)
1	–0.306V (I = 1.671) –0.719V (I = 1.620)	–0.321 (I = 1.892) –0.719 (I = 1.985)	–0.326 (I = 1.937) –0.719 (I = 2.161)
2	–0.314V (I = 1.509) –0.717V (I = 1.465)	–0.325 (I = 1.678) –0.717 (I = 1.746)	–0.321 (I = 1.649) –0.717 (I = 1.708)